Adsorption-Based Electrochemical Sensor Design for the Aqueous Detection of Paracetamol

*Pieter J. De Smedt, Aline Lauwers, Philippe M. Vereecken, Dirk E. De Vos, and Rob Ameloot**

This study investigates the critical role of adsorption in the development of electrochemical sensors, focusing on carbon (Vulcan XC72R, acetylene black, and graphite) and zeolite (high-silica ZSM-5 and all-silica zeolite β) materials. Based on the paracetamol adsorption characteristics of these materials, an optimized disposable electrochemical sensor is created. This sensor exhibits a linear range of up to 5 µM and a remarkable detection limit of 150 nM (S/N = 3), ≈1000-time improvement over the blank sensor. Moreover, paracetamol can be measured selectively because glucose has no adsorption affinity for the selected sensor materials. These findings underscore the significance of adsorption properties in sensor material selection in enhancing sensitivity and robustness against interfering species.

1. Introduction

The electrochemical detection of organic molecules in aqueous media offers low detection limits (nM range), fast measurement (seconds), and easy sample handling, often without pretreatment. For example, per- and poly-fluoroalkyl substances[1] and phenolic compounds can be detected electrochemically in surface water or wastewater.[2–4] In the food industry, electrochemical detection is employed for the determination of antibiotics in aquaculture wastewater.[5] In medicine, it facilitates monitoring health indicators like glucose levels (diabetes), uric acid levels (kidney function), and administered drug concentrations.[6–10]

The need for improved detection limits and selectivity has shifted the focus of electrochemical sensor research toward modified electrodes. Such electrodes are typically fabricated by drop casting, spin coating, or spray coating an ink composed of an adsorbent, a solvent, and binding agents like polytetrafluoroethylene[11] or polyvinylidene fluoride[12] onto the sensing electrode. Several adsorbents have been used, including carbon blacks,[13,14] carbon nanotubes,[4,15] zeolites,[16,17] metal–organic frameworks,[11,18,19] or combinations thereof. Intuitively, it is expected that coating an adsorbent onto an electrode will concentrate the analyte close to the sensing surface and result in improved electrode performance. However, to our surprise, we did not encounter any study that went beyond this intuitive explanation and tried to quantitatively relate the analyte uptake by the adsorbent to the resulting increase in the sensor signal.

In this study, we examined the relationship between the analyte affinity of adsorbents and their performance in electrochemical sensing. Paracetamol (PAR) was selected as the model analyte since it is one of the most widely used over-the-counter drugs[20] and a prevalent micropollutant in urban and industrial wastewater.[21,22] PAR residues are even found in drinking water due to the challenges of its removal during wastewater treatment processes,[22,23] underscoring the need for sensitive PAR sensors.

We selected three carbon materials and two zeolites as adsorbents. The carbon materials—graphite, acetylene black, and Vulcan XC72R—were chosen for their commercial availability, widespread use in electrode modification,[24–26] and expected affinity for aromatic compounds in an aqueous solution.[27,28] The selected zeolites were ZSM-5 with a 100:1 Si:Al ratio and all-silica zeolite β. Both zeolites have a high affinity for phenolic compounds because of their high silicon content.[29–31]

Since electrochemical PAR sensing is well established,[32–35] we use it here to illustrate how our approach—employing adsorption properties as a guiding principle in sensor design—enables the development of highly sensitive sensors that can rival existing standards. This adsorption-based methodology can be extended to other analytes.

2. Results and Discussion

2.1. Paracetamol Adsorption Isotherms

The adsorption isotherms of graphite (Gr), acetylene black (AB), Vulcan XC72R (Vu), all-silica zeolite β (β), and ZSM–5 (ZSM), shown in **Figure 1**, were determined by batch experiments at

P. J. De Smedt, A. Lauwers, P. M. Vereecken, D. E. De Vos, R. Ameloot
Center For Membrane Separations, Adsorption, Catalysis and Spectroscopy (cMACS)
KU Leuven
Celestijnenlaan 200F, box 2454, 3001 Leuven, Belgium
E-mail: rob.ameloot@kuleuven.be

P. M. Vereecken
Energy Department
Imec
Kapeldreef 75, 3001 Leuven, Belgium

P. M. Vereecken
Energyville
Thor Park 8320, 3600 Genk, Belgium

The ORCID identification number(s) for the author(s) of this article can be found under https://doi.org/10.1002/adem.202402051.

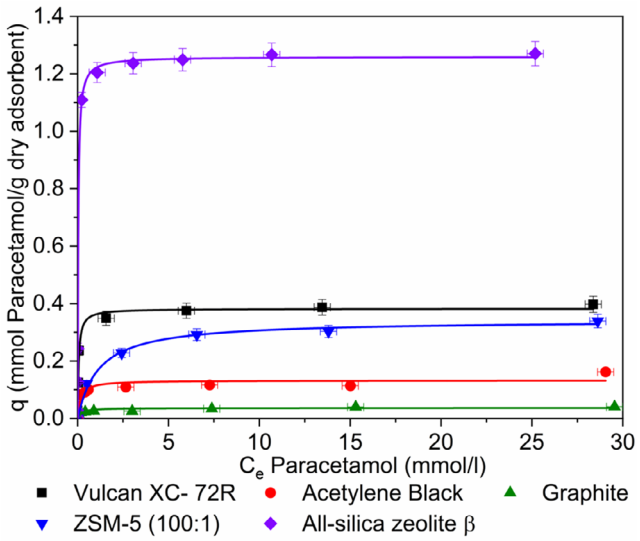

Figure 1. Paracetamol adsorption isotherms of Vulcan XC72R, acetylene black, graphite, zeolite ZSM-5 (100:1), and all-silica zeolite β. C_e is the equilibrium concentration after 24 h stirring at room temperature, and q is the amount adsorbed in mmol g^{-1} adsorbent at the equilibrium concentration. The isotherms were fitted using the Langmuir adsorption model. The q error indicates the standard deviation between two duplicate experiments measured for each isotherm point, and the C_e error indicates the standard deviation between three repeated HPLC measurements of the same stock PAR solution.

room temperature. The adsorbents were contacted with stock PAR solutions for 24 h, after which the remaining PAR concentration was determined via HPLC-UV analysis. Figure 1 shows the equilibrium concentration after 24 h on the x-axis and the amount adsorbed per mass adsorbent material on the y-axis. Figure S2, Supporting Information shows the adsorption isotherms at the lower concentration range (<0.5 mmol L^{-1}) in more detail.

The isotherm points were fitted using the Langmuir adsorption model (1), the fitting parameters of which are shown in **Table 1**. q is the amount adsorbed in mmol g^{-1} adsorbent at the equilibrium concentration, Q_{max} is the adsorption capacity for paracetamol, K_L is the Langmuir parameter, and C_e is the equilibrium concentration after 24 h stirring at room temperature. The fitting errors of the Langmuir parameters are shown in Table S6, Supporting Information

Table 1. Fitted Langmuir parameters for paracetamol adsorption isotherms, Q_{max} the adsorption capacity for paracetamol, K_L the Langmuir parameter.

	Q_{max} [mmol g^{-1}]	K_L [L $mmol^{-1}$]	χ^2	Adj. R^2
Vu	0.38	18.23	1×10^{-4}	0.99
AB	0.13	6.34	2×10^{-6}	0.99
Gr	0.037	5.42	5×10^{-8}	0.99
ZSM	0.34	0.87	1×10^{-6}	0.99
β	1.26	31.64	7×10^{-6}	0.99

$$q = \frac{Q_{max} K_L C_e}{1 + K_L C_e} \quad (1)$$

Meanwhile, the nitrogen physisorption isotherms are shown in Figure S5–S9 and Table S7, Supporting Information. The relationship between PAR adsorption capacity (Q_{max}) and the specific surface area determined by nitrogen physisorption (Brunauer–Emmett–Teller specific surface area, BET-SSA) is discussed in more detail in the Section 2.5, Supporting Information.

Besides Q_{max}, the other important model parameter is the Langmuir constant K_L, which indicates a material's affinity for an adsorbate; the higher the K_L, the stronger the affinity for PAR and the steeper the isotherm.[28] In the PAR concentration range most relevant for the sensor application (<1 mM), the best adsorbing carbon material is Vu, with a relatively high K_L of 18.23 L $mmol^{-1}$, compared with AB and Gr, with respective K_L values of 6.34 and 5.42 L $mmol^{-1}$. However, all carbons were outperformed by all-silica zeolite β, which had a K_L of 31.64 L $mmol^{-1}$, indicating a strong affinity for PAR. Interestingly, ZSM-5 had a much lower K_L (0.87 L $mmol^{-1}$), likely because of the presence of aluminum in the lattice compared to the all-silica nature of β.[31]

2.2. Sensor Coating Formulation and Sensor Fabrication

To integrate the different materials (Gr, AB, Vu, ZSM-5, and all-silica zeolite β), a suspension-based drop casting approach on a commercially available screen-printed electrode (SPE) was selected (**Figure 2**). The disposable SPEs are inexpensive (<2 euros per piece), and drop casting allows for fast production (more than 100 sensors per day in the lab). This combination allows for rapid testing of different coatings under different conditions, without the need for electrode cleaning or risk of cross contamination at a low cost, which is also ideal for commercial sensors.

Besides solids, the drop-casting suspension consisted of a solvent, binder, and surfactant, respectively water/ethanol, Nafion, and Surfynol 465. The surfactant proved a key factor in ensuring reproducible coatings by improving suspension stability and coating homogeneity during drying (Section 1.8, Supporting Information). Surfynol 465 was chosen because of its compatibility with water/alcohol solutions and proven success in carbon

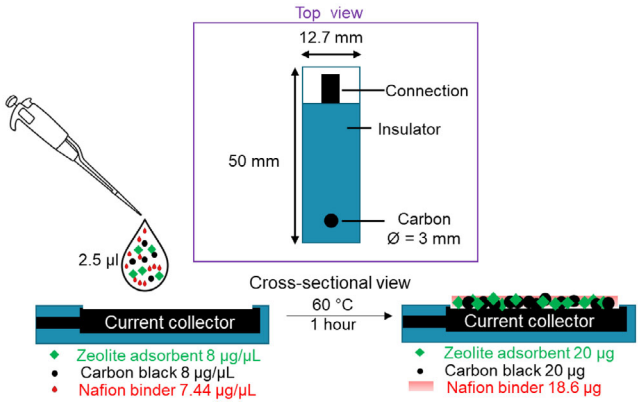

Figure 2. Schematic overview of the SPE and coating process.

ink formulation.[36–38] The Nafion loading was minimalized for every coating composition till the point that still allowed for reproducible coatings without (partial) detachment; in practice, the required loading was found to be proportional to the total mass of the suspended solids, independent of the type.

Based on the PAR isotherm results discussed above, the most promising sensor material would be all-silica zeolite β. However, the nonconductive nature of zeolites impedes a sensor purely based on zeolite, and thus, it must be paired with a conductive carbon to form a hybrid coating that allows electrochemical detection. Since the isotherms results (Figure 1) indicated Vu had the highest PAR affinity of the carbons, it was selected for the hybrid coatings. The optimal hybrid coating composition was determined by increasing the Vu loading in steps and then, at each step testing different carbon to zeolite ratios. The coating yielding the highest signal comprised 20 µg Vu + 20 µg zeolite. To more accurately compare the sensor coatings, the amount of carbon for all the coatings was fixed at 20 + 9.3 µg Nafion, and for the hybrid coatings, 20 µg Vu + 20 µg zeolite + 18.6 µg Nafion.

The top-view SEM image of the Vu + all-silica zeolite β (Vu + β) sensor in **Figure 3**A shows that the zeolite particles are evenly dispersed. The cross-sectional perspective, Figure 3B, reveals robust contact between the zeolite and carbon particles. Most likely, the zeolite particles act as channels, allowing more contact between the liquid and the carbon particles. The Supporting Information contains top-view SEM images of all sensor coatings (Table S8, Supporting Information), along with additional cross-sectional images for the Vu + all-silica zeolite β and Vu + ZSM-5 sensors (Table S9, Supporting Information) in Section 2.4, Supporting Information.

2.3. Electrochemically Active Surface Area of Sensor Coatings

Figure 4 shows the relationship between the experimentally determined electrochemically active surface area (EC-ASA) and the theoretical maximum, which would be the BET surface area of the carbon fraction. (Since the zeolites are nonconductive, they would not contribute to the EC-ASA.) For the blank, which was an uncoated SPE, the theoretical maximum was taken as the 2D flat surface area. Except for the blank, the EC-ASA values lie between the flat electrode area (0.07 cm^2) and the theoretical maximum (Figure 4). The lower EC-ASA for the blank, 0.03 cm^2 versus the flat surface area of 0.07 cm^2, is not

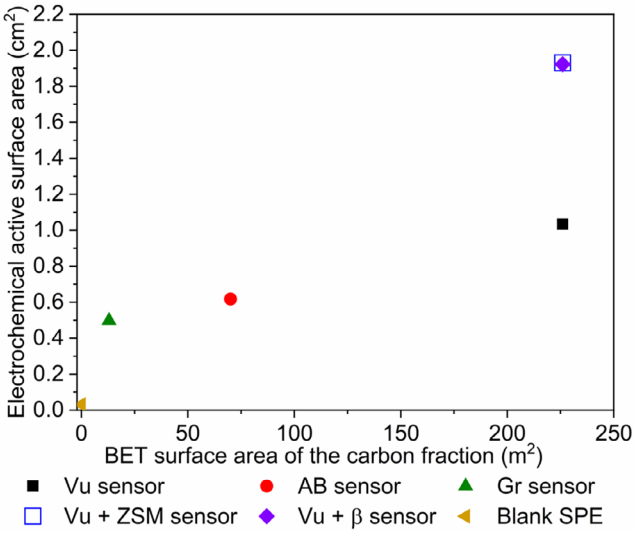

Figure 4. Experimentally determined electrochemically active surface area versus the theoretical maximal available surface area for each sensor and a blank SPE. Please note that the Vu + ZSM-5 sensor and Vu + all-silica zeolite β overlap.

uncommon for SPEs and is often attributed to the binders added in the manufacturing process that partially deactivate the surface.[39,40] The EC-ASAs of the three carbon-only sensors (Vu, AB, and Gr) followed a logical trend: the higher the BET-SSA of the material, the higher the EC-ASA. The Vu sensor had the highest EC-ASA of the three at 1.03 cm^2 (Figure 4). Interestingly, the Vu + zeolite sensors had much higher EC-ASAs of 1.92 and 1.93 cm^2 for Vu + all-silica zeolite β and Vu + ZSM-5, respectively (Figure 4); even though the conductive material, 20 µg of Vu, was the same, this could indicate that the addition of porous zeolites resulted in a larger liquid-carbon interface, thus allowing more Vu to be electrochemically active. Hence, besides the indented use of zeolite as an adsorbent for the compound of interest, it also positively affects the electrode coating's EC-ASA, which in turn can provide better sensor performance which will be taken into account for the interpretation of the electrochemical PAR sensing results. More details about the capacitance-based EC-ASA determination can be found in the Section 2.6, Figure S11–S13, and Table S10, Supporting Information.

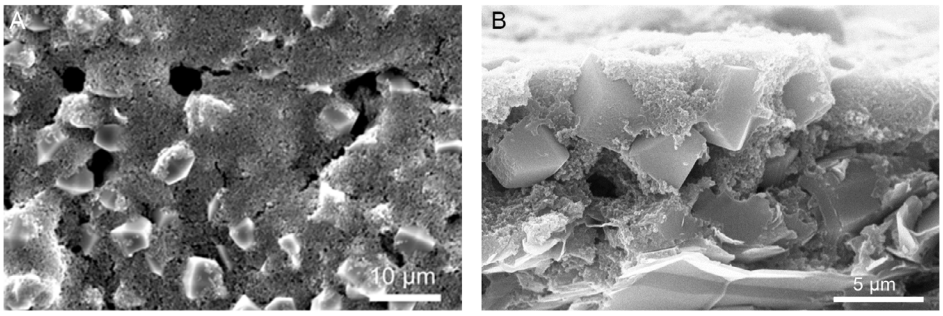

Figure 3. SEM image of the Vu + all-silica zeolite β sensor. A) Top view and B) Cross section.

2.4. Screening of Coating Inks

The electrode coatings were initially assessed by linear sweep voltammetry (LSV) using four stock PAR concentrations (1 mM, 100, 10, and 1 μM). Before the sensing measurements, the sensors were equilibrated with the PAR solution, which enhanced the signal by up to 40 times (Figure S14–S15, Section 2.7, Supporting Information). As more PAR molecules adsorb, the signal increases. The screening run offered valuable insight into the relative performance of the coatings relative to the PAR isotherm data. The lowest stock concentration for which all sensors could still measure a PAR oxidation peak was 100 μM. Sensors modified with Vu and AB could measure down to 10 μM, while those coated with Vu + all-silica zeolite β could detect the lowest concentration of 1 μM as well. **Figure 5** shows, for the stock concentration of 100 μM PAR, the LSV signals of all sensors on the left and the peak current on the right (Section 2.8, Supporting Information, Contains LSV scans of all concentrations). In Figure 5A, although the peak potentials of all sensors fell within a similar voltage range (350–400 mV versus Ag/AgCl), the peak potential for the blank SPE was shifted to 550 mV versus Ag/AgCl. This shift may be attributed to the binders incorporated during the SPE manufacturing process, which may partially deactivate the surface.[39,40]

As discussed in Section 2.1, Supporting Information, the adsorption behavior relevant to sensing PAR is largely governed by the Langmuir constant, K_L. The carbon-based sensors—Gr, AB, and Vu—displayed peak currents of 2.3, 2.9, and 4.7 μA, respectively, which aligned with their K_L values of 5.42, 6.34, and 18.23 L mmol^{-1}, as shown in Figure 5 and Table 1. Notably, sensors coated with zeolites outperformed all others: the Vu + ZSM-5 sensor achieved a peak current of 7.9 μA (70% enhancement versus 4.7 μA), and the Vu + all-silica zeolite β sensor reached a significantly higher peak current of 34.8 μA (710% enhancement versus 4.7 μA). Despite similar EC-ASAs (1.92 versus 1.93 cm^2), the two zeolites exhibited distinct PAR adsorption properties, with all-silica zeolite β showing a K_L of 31.64 L mmol^{-1} compared to ZSM-5's K_L of only 0.87 L mmol^{-1}. The total gain of the Vu + all-silica zeolite β sensor is 3250% compared to the blank SPE (34.8 versus 1.07 μA). These findings align with the adsorption isotherm data, reinforcing that Vu, the carbon with the highest adsorption affinity, also demonstrates the best sensor performance. Moreover, incorporating highly PAR-adsorbing all-silica zeolite β further enhances the sensor's performance, while the effect of the lower-adsorbing ZSM-5 remains relatively limited.

2.5. Limit of Detection, Linear Range, Reusability, and Fabrication Repeatability for the Vu + All-Silica Zeolite β Sensor

The measurement conditions for the best-performing sensor of the screening experiment, the Vu + all-silica zeolite β sensor, were further optimized with an activation step (voltage cycling the fabricated electrode first in a 0.1 M phosphate buffer solution), and the pre-equilibration step was reduced to 5 min in a stirred solution. (Additional information can be found in Section 2.7, Supporting Information). **Figure 6** illustrates the linear sweeps and calibration curve of the Vu + all-silica zeolite β sensor. A linear range of up to 5 μM, along with a LOD of 150 nM (S/N = 3), was achieved.

The Vu + all-silica zeolite β sensor also shows excellent reusability for PAR sensing. By repeating the same sensing protocol, the sensor could be reused with only a maximum peak current shift of 6% between the fresh and three times used sensors (Section 1.10.5 and 2.9, Supporting Information). All measurements used to create the calibration line in Figure 6 were done with freshly fabricated electrodes (each point and each repeat) with only a small degree of error. For analytes more prone to fouling, such as phenol,[41,42] a single-use approach would be preferable and possible using the inexpensive fabrication protocol of this work (<2 euros per sensor).

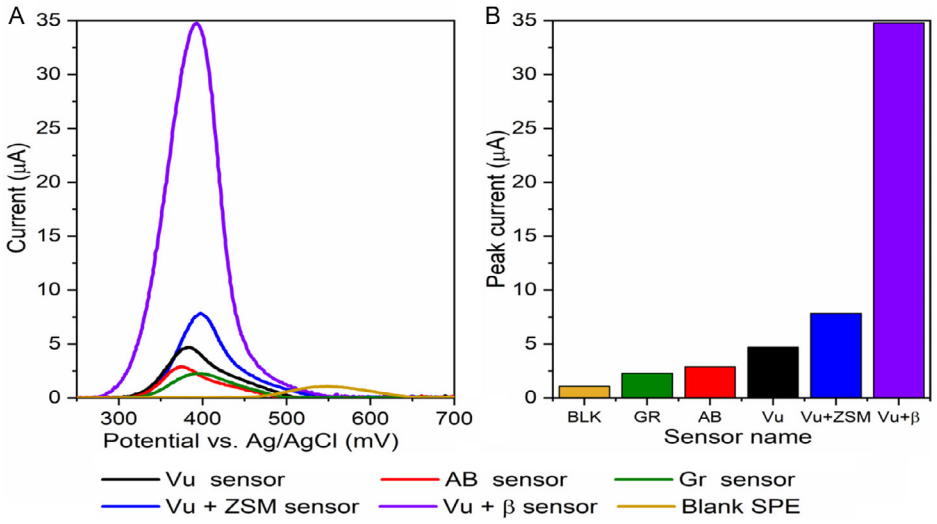

Figure 5. For 100 μM paracetamol, A) linear sweep scans of all sensors and blank SPE and B) the corresponding anodic peak currents of the linear sweep scans; experiments were performed in 0.1 M aqueous phosphate buffer solution, pH 7 with a scan speed of 50 mV s^{-1}, a counter electrode Pt plate, and reference electrode Ag/AgCl.

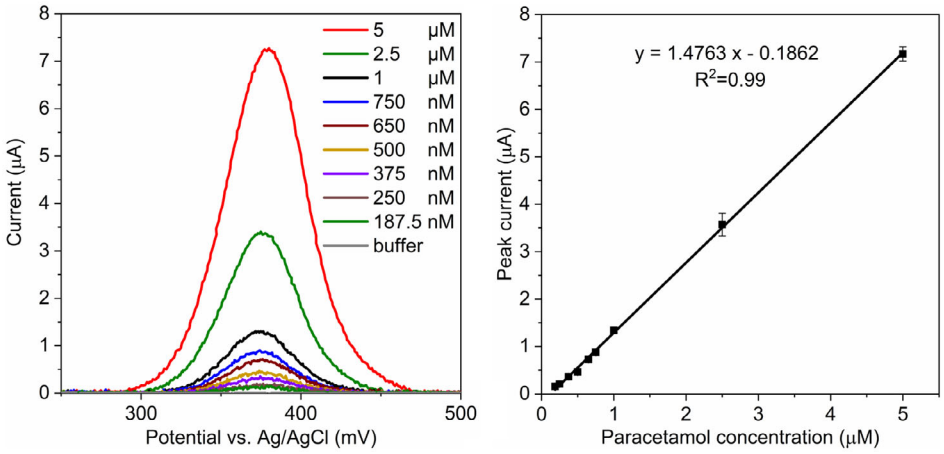

Figure 6. Linear sweep scans of the Vu + all-silica zeolite β sensor and resulting calibration curve for PAR detection; experiments were performed in 0.1 M aqueous phosphate buffer solution, pH 7 with a scan speed of 50 mV s^{-1}, a counter electrode Pt plate, and reference electrode Ag/AgCl.

Although this is not explicitly mentioned in the sources, the work of other PAR sensors mentioned in **Table 2** can often be categorized as having taken either a more adsorption approach (such as the Vu + all-silica zeolite β sensor) or a more catalytic approach to improved sensor performance. In the former case, such as single-wall carbon nanotubes,[43] and polyimide–multiwall carbon nanotubes,[44] a PAR adsorbing material is added to the base electrode material; in the latter case of BiVO,[45] and NiO,[6] a more catalytic/reactive electrode material is added. Meanwhile, the iron oxide encapsulated in chitosan-grafted-polyaniline,[46] Ni zeolite with graphene oxide,[47] and cobalt oxide–embedded nitrogen-doped hollow carbon spheres[48] can be seen as a combination of adsorption and catalytic approach. While the Vu + all-silica zeolite β sensor, with its detection limit of 150 nM, is not the best-performing PAR sensor in recent literature (Table 2), it does outperform the other sensors of Table 2, including Ni zeolite + GO[47] sensor and Co_3O_4@NHCS[48] reaching respective detection limits of 7.8 and 70 nM. Additionally, the Vu + all-silica zeolite β sensor is based on an affordable disposable electrode and a straightforward detection method involving LSV, while the Ni zeolite + GO[47] and the Co_3O_4@NHCS[48] sensor are more difficult to fabricate/nondisposable and use differential pulse voltammetry (DPV) as a detection method. Potentiostats capable of LSV measurements are available for under €100.[49,50] In contrast, DPV is a more complex method and often requires a more expensive measurement setup (>€850, e.g., PalSens Sensit).[51,52] Hence, the Vu + all-silica zeolite β sensor provides a practical, affordable, and highly sensitive PAR detection platform.

Table 2. Overview of sensor's performance compared with the literature.

Sensor material	Current collector	LOD	Detection method	(Year) source
Vu + all-silica zeolite β	SPE	150 nM	LSV	This work
SWCNTs[a)]	SPE	819 nM	DPV	[43]
$BiVO_4$	FTO[f)]	200 nM	DPV	[45]
PI-MWCNT[b)]	Pt	2000 nM	DPV	[44]
α-Fe_2O_3-en-CHIT-g-PANI[c)]	ITO[g)]	5700 nM	Potentiometric	[46]
Ni zeolite + GO[d)]	CPE[h)]	7.8 nM	DPV	[47]
NiO	GC[i)]	230 nM	DPV	[6]
Co_3O_4@NHCS[e)]	GC	70 nM	DPV	[48]

[a)]Single-wall carbon nanotubes. [b)]Polyimide–multiwall carbon nanotubes. [c)]Iron oxide encapsulated in chitosan-grafted-polyaniline. [d)]Nickel zeolite with graphene oxide. [e)]Cobalt oxide–embedded nitrogen-doped hollow carbon spheres. [f)]Fluorine-doped tin oxide. [g)]Indium tin oxide. [h)]Carbon paste electrode. [i)]Glassy carbon.

2.6. PAR versus Glucose Selectivity

In addition to enhancing sensitivity, adsorption characteristics can also guide the enhancement of sensor selectivity. To demonstrate this, glucose was chosen as a potential interference source for PAR sensing. If the Vu + all-silica zeolite β sensor were applied to analyze blood samples, glucose would be present, and though not the same molecular type as PAR, carbon electrodes have been reported to oxidize glucose in 0.1–0.6 V[53–55] range (the Vu + all-silica zeolite β sensor PAR oxidation peak occurs at 375 mV; hence, glucose could be a potential interferent. Typical fasting blood glucose levels range between 5.6 and 6.9 mM.[56] Glucose adsorption was assessed for Vu and all-silica zeolite β across a concentration range of 1 to 30 mM (Figure S19, Supporting Information), with no detectable adsorption observed for either material. Consistent with these results, the Vu + all-silica zeolite β sensor electrochemical exhibited no response to glucose, even at a concentration as high as 10 mM (Figure S20, Supporting Information).

Consequently, glucose presence does not interfere with PAR detection, as depicted in **Figure 7**A, which presents an example LSV scan of a PAR signal both with and without 10 mM glucose in solution. Figure 7B presents the calibration curve of the Vu + all-silica zeolite β sensor for PAR sensing with 10 mM glucose in solution. Comparison of this curve with Figure 6 reveals that glucose does not impede PAR sensing; the PAR LOD remained at 150 nM (S/N = 3), and the curve equation showed only slight deviation, $y = 1.4588x - 0.1937$ versus $y = 1.4763x - 0.1862$.

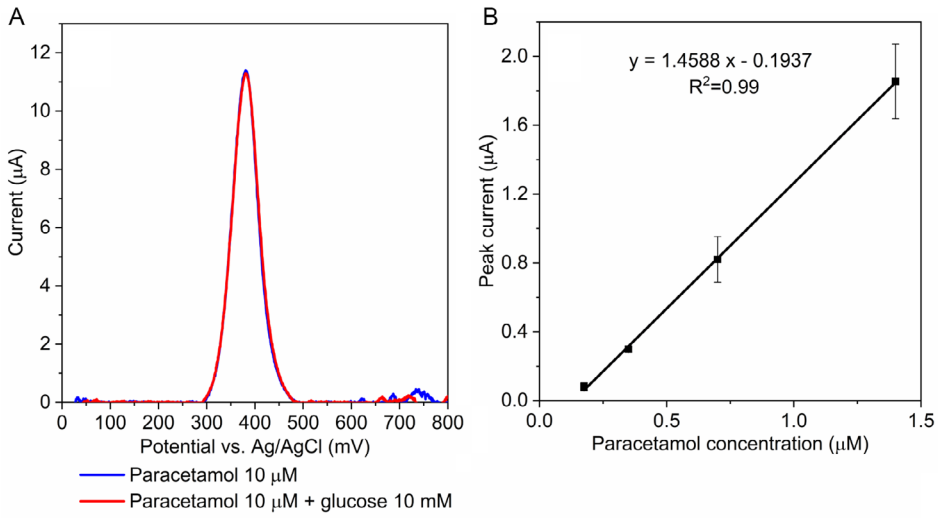

Figure 7. Influence of glucose on paracetamol detection for the Vu + all-silica zeolite β sensor. A) Example linear sweep scans for paracetamol (blue) and paracetamol in the presence of glucose (red). B) A calibration curve for paracetamol detection in the presence of 10 mM glucose. Scan speed 50 mV s^{-1}, counter electrode Pt plate, and reference electrode Ag/AgCl. Measurements were performed in 0.1 M aqueous phosphate buffer solution, pH 7.

3. Conclusion

By systematically investigating the adsorption properties of various carbon and zeolite materials, we rationalized their performance in sensor electrodes. The disposable PAR sensor constructed based on these insights demonstrated a remarkable detection limit of 150 nM (S/N = 3). Moreover, the absence of glucose adsorption on Vu and all-silica zeolite β clarified how PAR can be detected selectively in the presence of glucose. The study showed how adsorption properties can provide guidance to achieve both sensor sensitivity and selectivity.

Supporting Information

Supporting Information is available from the Wiley Online Library or from the author.

Acknowledgements

P.J.D.S. thanks FWO Flanders for a doctoral fellowship (1SB5121N/1SB5119N) and the Cabot company for providing a Vulcan XC72R sample. The authors acknowledge funding from VLAIO in projects HBC.2020.2615 and HBC.2021.0580.

Conflict of Interest

The authors declare no conflict of interest.

Author Contributions

Pieter J. De Smedt: Conceptualization (equal); Data curation (lead); Formal analysis (lead); Funding acquisition (equal); Investigation (lead); Methodology (equal); Project administration (equal); Validation (lead); Visualization (lead); Writing—original draft (lead). **Aline Lauwers**: Formal analysis (supporting); Investigation (supporting); Methodology (supporting). **Philippe M. Vereecken**: Conceptualization (supporting); Formal analysis (supporting); Investigation (supporting); Methodology (equal); Validation (supporting). **Dirk E. De Vos**: Conceptualization (supporting); Formal analysis (supporting); Funding acquisition (equal); Investigation (supporting); Methodology (supporting); Project administration (supporting); Resources (equal); Supervision (supporting). **Rob Ameloot**: Conceptualization (equal); Funding acquisition (equal); Methodology (equal); Project administration (equal); Resources (lead); Supervision (lead); Writing—review & editing (lead).

Data Availability Statement

The data that support the findings of this study are available in the supplementary material of this article.

Keywords

adsorptions, carbon blacks, disposable electrodes, electrochemistry, modified electrodes, paracetamol

Received: September 2, 2024
Revised: October 31, 2024
Published online:

[1] R. B. Clark, J. E. Dick, *ACS Sens.* **2020**, *5*, 3591.
[2] W. Qin, X. Liu, H. Chen, J. Yang, *Anal. Methods* **2014**, *6*, 5734.
[3] Y. Wang, J. Qu, S. Li, Y. Dong, J. Qu, *Microchim. Acta* **2015**, *182*, 2277.
[4] L. A. Goulart, R. Gonçalves, A. A. Correa, E. C. Pereira, L. H. Mascaro, *Microchim. Acta* **2017**, *185*, 12.
[5] Y. Liu, J. Chen, H. Hu, K. Qu, Z. Cui, *Int. J. Environ. Res. Public Health* **2022**, *19*, 16945.
[6] K. Annadurai, V. Sudha, G. Murugadoss, R. Thangamuthu, *J. Alloys Compd.* **2021**, *852*, 156911.
[7] M. Roushani, F. Shahdost-fard, *Talanta* **2015**, *144*, 510.
[8] A. Wong, A. M. Santos, F. H. Cincotto, F. C. Moraes, O. Fatibello-Filho, M. D. P. T. Sotomayor, *Talanta* **2020**, *206*, 120252.

[9] H. Yoon, J. Nah, H. Kim, S. Ko, M. Sharifuzzaman, S. C. Barman, X. Xuan, J. Kim, J. Y. Park, *Sens., Actuators B* **2020**, *311*, 127866.
[10] J. Liu, X. Jiang, R. Zhang, Y. Zhang, L. Wu, W. Lu, J. Li, Y. Li, H. Zhang, *Adv. Funct. Mater.* **2019**, *29*, 1807326.
[11] H. Guo, T. Fan, W. Yao, W. Yang, N. Wu, H. Liu, M. Wang, W. Yang, *Microchem. J.* **2020**, *158*, 105262.
[12] Y. Xing, G. Gao, G. Zhu, J. Gao, Z. Ge, H. Yang, *J. Electrochem. Soc. B* **2014**, *161*, 106.
[13] M. M. Lounasvuori, D. Kelly, J. S. Foord, *Carbon* **2018**, *129*, 252.
[14] T. A. Silva, B. C. Lourencao, A. Dias Da Silva, O. Fatibello-Filho, *Anal. Methods* **2023**, *15*, 1077.
[15] M. Irfan, A. Shah, F. J. Iftikhar, M. Hayat, M. N. Ashiq, I. Shah, *ACS Omega* **2022**, *7*, 32302.
[16] R. Porada, K. Fendrych, B. Baś, *Microchim. Acta* **2021**, *188*, 323.
[17] A. H. Miller, H. T.-T. Nguyen, J. G. Nery, A. J. Fielding, *J. Appl. Electrochem.* **2023**, *53*, 1715.
[18] X. Wang, Q. Wang, Q. Wang, F. Gao, F. Gao, Y. Yang, H. Guo, *ACS Appl. Mater. Interfaces* **2014**, *6*, 11573.
[19] X. Chen, Y. Li, X. Li, R. Li, B. Ye, *Anal. Chim. Acta.* **2022**, *1209*, 338992.
[20] C. V. Sharma, V. Mehta, *Contin. Educ. Anaesth. Crit. Care Pain* **2014**, *14*, 153.
[21] J. Żur, A. Piński, A. Marchlewicz, K. Hupert-Kocurek, D. Wojcieszyńska, U. Guzik, *Environ. Sci. Pollut. Res.* **2018**, *25*, 21498.
[22] S. Wu, L. Zhang, J. Chen, *Appl. Microbiol. Biotechnol.* **2012**, *96*, 875.
[23] J.-S. Rhee, B.-M. Kim, C.-B. Jeong, H. G. Park, K. M. Y. Leung, Y.-M. Lee, J.-S. Lee, *Comp. Biochem. Physiol., Part C* **2013**, *158*, 216.
[24] A.-N. Kawde, N. Baig, M. Sajid, *RSC Adv.* **2016**, *6*, 91325.
[25] S. Sun, X. Xu, A. Niu, Z. Sun, Y. Zhai, S. Li, C. Xuan, Y. Zhou, X. Yang, T. Zhou, Q. Tian, *Int. J. Electrochem. Sci.* **2022**, *17*, 221187.
[26] R. M. Abdel Hameed, *Biosens. Bioelectron.* **2013**, *47*, 248.
[27] J. A. Mattson, H. B. Mark, M. D. Malbin, W. J. Weber, J. C. Crittenden, *J. Colloid Interface Sci.* **1969**, *31*, 116.
[28] H. N. Tran, S.-J. You, A. Hosseini-Bandegharaei, H.-P. Chao, *Water Res.* **2017**, *120*, 88.
[29] L. Damjanović, V. Rakić, V. Rac, D. Stošić, A. Auroux, *J. Hazard. Mater.* **2010**, *184*, 477.
[30] Y. Liu, H. Lu, *Mater. Res. Express* **2020**, *7*, 055506.
[31] M. Van den Bergh, A. Krajnc, S. Voorspoels, S. R. Tavares, S. Mullens, I. Beurroies, G. Maurin, G. Mali, D. E. De Vos, *Angew. Chem., Int. Ed.* **2020**, *59*, 14086.
[32] J. Hoq, M. F. Islam, M. R. Miah, M. M. Rahman, A. Almahri, M. A. Hasnat, *J. Environ. Chem. Eng.* **2022**, *10*, 108141.
[33] W. Boumya, N. Taoufik, M. Achak, N. Barka, *J. Pharm. Anal.* **2021**, *11*, 138.
[34] A. Cernat, M. Tertiş, R. Săndulescu, F. Bedioui, A. Cristea, C. Cristea, *Anal. Chim. Acta* **2015**, *886*, 16.
[35] Ž.Z. Tasić, M. B. Petrović Mihajlović, A. T. Simonović, M. B. Radovanović, M. M. Antonijević, *Results Phys.* **2021**, *22*, 103911.
[36] https://www.coatino.com/products/PR_52041345 (accessed: 4th August 2024).
[37] C. Yoon, J.-H. Choi, *Color. Technol.* **2020**, *136*, 60.
[38] C.-H. Kuo, J.-W. Shiu, S.-P. Rwei, *Colloids Surf., A* **2022**, *648*, 129450.
[39] X. Yuan, L. Ma, J. Zhang, Y. Zheng, *Appl. Surf. Sci.* **2021**, *544*, 148760.
[40] P. Fanjul-Bolado, P. Queipo, P. Lamasardisana, A. Costagarcia, *Talanta* **2007**, *74*, 427.
[41] S. Deheryan, D. J. Cott, R. Muller, M. Timmermans, M. Heyns, P. M. Vereecken, *Carbon* **2015**, *88*, 42.
[42] M. Y. Timmermans, F. Mattelaer, S. Moitzheim, N. Clerckx, A. Sepulveda, S. Deheryan, C. Detavernier, P. M. Vereecken, *J. Appl. Polym. Sci.* **2017**, *134*, 44533.
[43] N. Wester, B. F. Mikladal, I. Varjos, A. Peltonen, E. Kalso, T. Lilius, T. Laurila, J. Koskinen, *Anal. Chem.* **2020**, *92*, 13017.
[44] M. Burç, S. Köytepe, S. T. Duran, N. Ayhan, B. Aksoy, T. Seçkin, *Measurement* **2020**, *151*, 107103.
[45] Y. Liu, X. Xu, C. Ma, F. Zhao, K. Chen, *Nanomaterials* **2022**, *12*, 1173.
[46] C. S. Kushwaha, S. K. Shukla, *ACS Appl. Polym. Mater.* **2020**, *2*, 2252.
[47] R. Porada, N. Wenninger, C. Bernhart, K. Fendrych, J. Kochana, B. Baś, K. Kalcher, A. Ortner, *Microchem. J.* **2023**, *187*, 108455.
[48] V. Duraisamy, V. Sudha, V. Dharuman, S. M. Senthil Kumar, *ACS Biomater. Sci. Eng.* **2023**, *9*, 1682.
[49] S. Sarkar, M. Bhattacharya, in *The 46th Annual Conf. of the IEEE Industrial Electronics Society (IECON 2020)*, Singapore **2020**.
[50] A. A. Rowe, A. J. Bonham, R. J. White, M. P. Zimmer, R. J. Yadgar, T. M. Hobza, J. W. Honea, I. Ben-Yaacov, K. W. Plaxco, M. Wanunu, *PLoS One* **2011**, *6*, e23783.
[51] https://maciassensors.com/product/anapot-usb-potentiostat/ (accessed: 15th December 2023).
[52] https://maciassensors.com/differential-pulse-voltammetry/ (accessed: 8th December 2023).
[53] G. Wang, X. He, L. Wang, A. Gu, Y. Huang, B. Fang, B. Geng, X. Zhang, *Microchim. Acta* **2013**, *180*, 161.
[54] J. Wang, X. Sun, X. Cai, Y. Lei, L. Song, S. Xie, *Electrochem. Solid-State Lett.* **2007**, *10*, J58.
[55] J.-S. Ye, Y. Wen, W. De Zhang, L. Ming Gan, G. Q. Xu, F.-S. Sheu, *Electrochem. Commun.* **2004**, *6*, 66.
[56] https://www.who.int/data/gho/indicator-metadata-registry/imr-details/2380 (accessed: 12th December 2023).